Performance optimization of active quenching circuits for picosecond timing with single photon avalanche diodes

A. Lacaita, S. Cova, C. Samori, and M. Ghioni
Politecnico di Milano, Dipartimento di Elettronica e Informazione and CEQSE-CNR, Piazza L. da Vinci 32, Milano 20133, Italy

(Received 3 January 1995; accepted for publication 16 May 1995)

The front-end electronic circuitry plays a fundamental role in determining the performance obtained from ultrafast and highly sensitive photodetectors. In this paper we deal with electronic problems met working with single photon avalanche diodes for detecting single optical photons and measuring their arrival time with picosecond resolution. We describe an active quenching circuit capable of driving the detector in a remote position, connected with a coaxial cable. By minimizing the noise of the input stage we succeeded in reducing the contribution of the detector circuitry to the measured time resolution to less than 10 ps full width at half-maximum. © *1995 American Institute of Physics.*

I. INTRODUCTION

Since the advent of synchronously pumped dye lasers, ultrafast optical pulses have become readily available and time correlated photon counting (TCPC) has gained wide acceptance as an experimental technique for studying luminescence and fluorescence in chemistry, biology, physics, and material science. Figure 1 shows a typical TCPC setup in which a luminescence pulse from a sample is excited by a picosecond laser pulse. The luminescence pulse is attenuated by suitable neutral density filters, so that no more than one photon per pulse reaches the detector area. The time delay between the emission of the light pulse and the detection of the photon is measured with a time to pulse height converter (TPHC). This module is triggered on the start input by an electrical signal synchronous with the emission of the light pulse and on the stop input by the signal from the detector electronics module. The output of the TPHC is a voltage pulse with an amplitude proportional to the time delay between start and stop triggers. A multichannel analyzer digitizes the TPHC output and collects the histogram of many similar measurements. This histogram is the convolution between the actual shape of the light pulse and the instrumental response of the apparatus. The latter response sets the minimum duration of the measurable optical signal; its full width at half-maximum (FWHM) is also referred to as instrumental timing resolution and is given by the quadratic composition of the following contributions:

(a) the FWHM time jitter of the start pulse to the TPHC with respect to the onset of the light pulse;
(b) the FWHM timing resolution of the single photon detector, that is the FWHM jitter between the true arrival time of the photon and the detector pulse;
(c) the FWHM of the additional jitter introduced by the detector circuitry;
(d) the FWHM due to the noise and the short-term drift of the TPHC.

Only two types of detectors reach single photon sensitivity and subnanosecond time resolution: Photomultiplier tubes (PMTs) and single photon avalanche diodes (SPADs). The ordinary fast PMTs, with electrostatically focused, discrete dynode multiplier, have resolution values ranging from 600 to 120 ps FWHM. Similar results are found among silicon SPADs. The time resolution of reach through, high quantum efficiency devices ranges from about 320 ps FWHM of the EG&G/RCA C30902S, to 168 ps FWHM of the EG&G SLIK.[1,2] The first shallow junction SPADs, demonstrated at the beginning of the 1980s, attain timing performance of about 70 ps FWHM.[3]

As long as these detectors are employed, the timing performance of the TCPC apparatus is limited by the detector performance. In fact the start signal for the TPHC may be derived from the RF wave form driving the modulator in the mode-locked laser cavity. This signal is fed to a fast discriminator in order to shape standard pulses for the TPHC. Another alternative is to split off part of the laser beam onto a fast *p-i-n* photodiode. However, since the amplitude of the laser pulse may change by about 5%–10%, the *p-i-n* signal must be fed to a constant fraction trigger (CFT) in order to derive a standard pulse for the TPHC and minimize the time jitter. In both cases, the contribution (a) can be easily reduced to about 25 ps FWHM. Regarding the detector circuitry, the conventional CFTs for PMTs may introduce an additional jitter of 20 ps FWHM,[4] while the jitter of active quenching circuits (AQCs) for SPADs was about 15 ps FWHM.[5] Finally the contribution (d), due to the TPHC is usually less than 10 ps FWHM. Therefore, the quadratic composition of (a), (c), and (d) gives 30–35 ps FWHM, well below the value of the intrinsic performance of the detector.

However, in recent years, reliable ultrafast microchannel plate PMTs have become commercially available and detector resolution of 20 ps FWHM has been reported.[6] The same result has been demonstrated for specifically designed SPADs fabricated with a shallow depletion layer and small active area (5 μm diam).[5] In order to fully exploit this timing performance further care must be devoted to reduce the electronic jitter. By careful setting both the laser and the electronics the contribution (a) can be usually reduced down to 15 ps FWHM. Criteria for optimum selection of the preamplifier following ultrafast multichannel plate (MCP) PMTs have been discussed in a previous paper[4] and a new CFT for

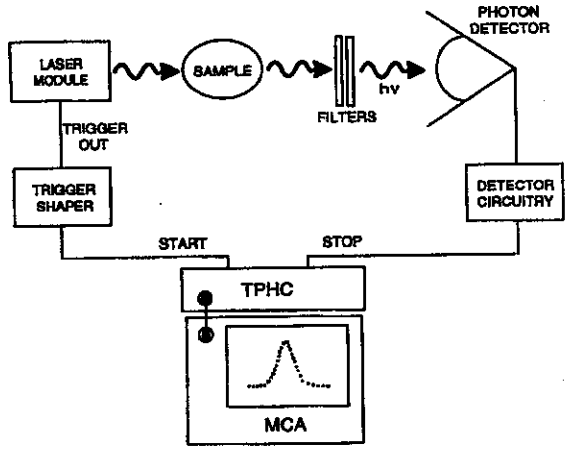

FIG. 1. A typical TCPC apparatus.

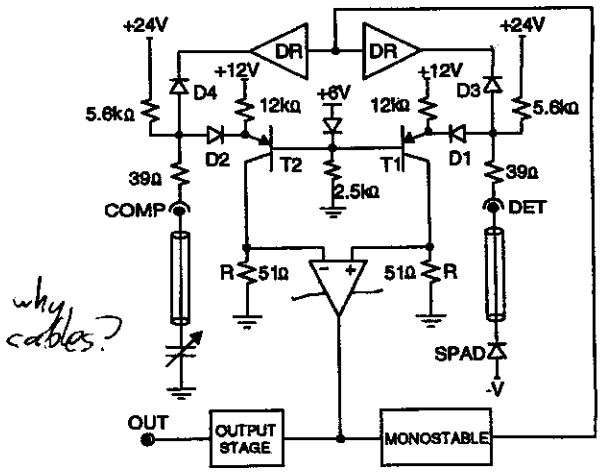

FIG. 2. Schematic of the AQC. The DET and COMP inputs are symmetrically loaded with the SPAD and with a compensation capacitor sets to a value equal to the SPAD capacitance. The quenching driver (DR) is a discrete push–pull stage, and the discriminator is the SP9685.

MCP PMTs with picosecond residual walk has been designed.[7] In this work we analyze limitations met working with fast SPADs. We first describe an AQC capable of driving the detector in a remote position, connected with a coaxial cable. We then discuss an AQC input stage specifically designed to minimize the circuit noise. We succeeded in reducing the jitter of the detector circuitry to less than 10 ps FWHM.

II. ACTIVE QUENCHING CIRCUITS

SPADs have a peculiar operation, fundamentally different from that of PMTs, and of ordinary avalanche photodiodes (APDs). The device does not have a linear internal gain, that is, it does not linearly amplify the primary photocurrent. It instead exploits the avalanche process to behave in a way similar to that of a trigger circuit, rather than an amplifier. In their operation, an external circuit drives the SPAD bias above the breakdown voltage, V_b, of the sensitive junction. At this bias the first carrier generated in the detector triggers a diverging avalanche process. The resulting current pulse has a rise time in the nanosecond range and reaches an amplitude given by the ratio between the excess bias above V_b and the diode series resistance. If the first carrier has been generated by photon absorption, the current leading edge marks very precisely the photon arrival time.

In early studies on SPADs, it soon became clear that the best timing performance is obtained by operating the SPAD with AQCs.[3,8,9] In these circuits three sections with different functional tasks may be identified:

(i) the input stage, where a fast discriminator senses the onset of the avalanche current, thus generating an output pulse synchronous with the avalanche and available for the following timing electronics.

(ii) a voltage driver, which lowers the bias voltage of the diode below V_b as soon as the avalanche is sensed. The driver must have a low-impedance output, capable of driving the capacitance associated with the SPAD and its connections.

(iii) a hold-off controller, which is usually built with monostables, triggered by the output of the fast discriminator. This section carefully defines the duration of the voltage pulse which lowers the detector bias below V_b after each avalanche. After the hold-off time, the circuit restores the initial bias so that the diode is again ready to detect a subsequent photon.

Various requirements must be satisfied for obtaining a correct AQC operation. One problem in particular is caused by the large amplitude difference between the avalanche pulse generated by the SPAD and the much larger voltage pulse that quenches the detector avalanche. This pulse has an amplitude up to several tens of volts and is delivered to the detector connected to the circuit input. Therefore, the input stage of the AQC should be sensitive to avalanche pulses of less than 1 mA (<50 mV over 50 Ω), but insensitive to quenching pulses. Due to the ringings and overshoots on the resetting transition of the quenching pulse, special precautions have been taken in the circuit design in order to avoid a false triggering of the AQC, that would end up in a self-sustained oscillation. RF coupling between high speed large voltage pulses and the timing discriminator is usually minimized by placing the discriminator inputs far from the driver.

In our laboratory, various generations of AQC have been developed, starting in 1975 from the earliest simple model[9] and progressively increasing the performance by a steady evolution of the design. Such evolution has produced an AQC design that provides remarkable flexibility for different applications and can work with a SPAD in a remote position, connected by a coaxial cable. It can work at more than 10 MHz repetition rate and, with suitably designed output quenching driver, it can provide a 40 V quenching pulse. The circuit design approach, covered by international patents,[10] will be here illustrated making reference to the simplified circuit diagram in Fig. 2.

Figure 2 highlights the high degree of symmetry of the circuit input stage, with the fast discriminator. In quiescent conditions a bias current of 3 mA flows through the diodes D_1 and D_2, while diodes D_3 and D_4 are off. A simple resistive

how to implement without adversely affecting symmetry?

voltage divider, not shown in Fig. 2, keeps the inverting input of the discriminator biased about 15 mV below the noninverting one, thus setting the discriminator threshold level. When an avalanche is triggered, the avalanche signal flows through the diode D_1 and the common-base transistor T_1, reaching the 51 Ω resistor, R, at the discriminator input. The avalanche pulse is applied asymmetrically (only to the noninverting terminal of the discriminator), thus being a differential signal for the discriminator. As soon as the avalanche current overcomes the threshold level of 300 μA=15 mV/51 Ω, the discriminator output changes state, thus triggering the quenching driver DR, a simple push–pull output stage assembled with discrete components. The quenching voltage pulse generated by DR, makes D_3 conducting and is delivered to the SPAD. At the same time the diode D_1 is driven to reverse bias condition and prevents the high voltage pulse from reaching T_1. If the diodes D_1, D_2 were not present, the entire quenching pulse would be applied to the base-emitter junction of T_1 (and T_2), causing it to breakdown.

The discriminator employed in our circuits was an ECL integrated circuit, SP9685, specified for a typical propagation delay of 2.2 ns. Its input resistance is 60 kΩ, while the stray capacitance from each input to ground is about 4 pF. The integrated circuit, designed as a cascade of ECL differential stages, has a small signal bandwidth of about 300 MHz.[11]

The detector is held off for an accurately controlled time, set by the monostable. The actual value of the hold-off time can be very short, a few tens of nanoseconds or less, in cases where photons have to be counted at high rate, up to 10 MHz or more. However, in cases where photon arrival times must be accurately measured and the dark count rate must be minimized, a somewhat longer hold-off time has to be employed, typically a few hundred nanoseconds, in order to avoid SPAD retriggering due to the delayed release of trapped carriers. At the end of the hold-off time the bias is raised above V_b.

Due to the high impedance of the detector, both the quenching and the resetting transitions of the quenching voltage pulse are reflected back to the circuit input when they reach the SPAD. Further reflections at the circuit are avoided by the 50 Ω termination, given by the series of a 39 Ω resistor with the common base input resistance, in series with the cable. However, it is worth noting that the reflected signal due to the quenching transition reaches the circuit when the diodes D_1 and D_2 are already off. In this case the discriminator inputs are decoupled from the driver and the discriminator is at stand-by, with the inverting input biased 15 mV below the noninverting one. On the contrary, when the resetting pulse, reflected by the SPAD, reaches the AQC input, the diodes D_1 and D_2 are recovering their conducting state. Therefore, reflections, overshoots, or ringing may cause the voltage of the noninverting input of the discriminator to be lowered below that of the inverting one. In this case, the discriminator is triggered and the driver DR lowers again the detector bias below V_b. Since the same ringing will always occur and trigger the discriminator on each resetting transition, the circuit becomes self-triggering, breaks into oscillations, and is useless for driving the detector. In order to avoid such behavior, the noninverting input of the AQC must

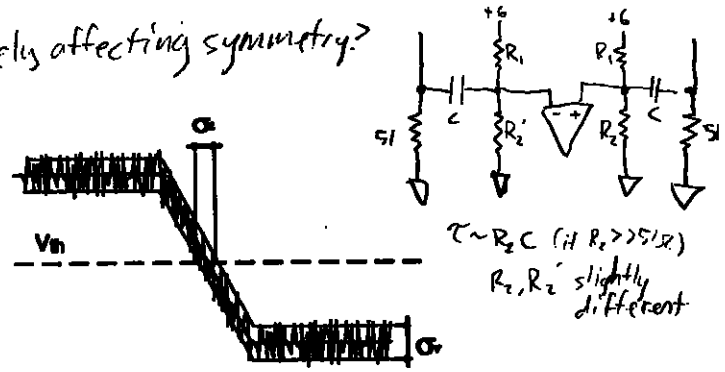

FIG. 3. Time jitter of the threshold crossing due to the discriminator input noise.

be connected with a coaxial cable having the same length, to a passive load matching the impedance of the SPAD. In this way the two branches are perfectly symmetric and no differential signals are generated at the discriminator inputs also during the voltage transients, even in the presence of ringings due to stray inductances. Thanks to the symmetry of the input stage, the fast comparator can work with a 15 mV threshold level, as required to sense the avalanche pulse, and at the same time be insensitive to the common mode quenching pulses. In practice, a satisfactory balance between the two inputs of the circuit is easily obtained by using as the passive load a trimmer capacitor of a few pF, which is set to a capacitance value approximately equal to that of the SPAD. The flexibility and performance of the circuit have been extensively tested in many different experiments, carried out in a wide variety of conditions, with the SPAD working either embedded in the circuit or remote from it, within a microscope or even in a cryostat.[12]

III. ELECTRONIC TIME JITTER

The time jitter of the AQC may arise from the electronic noise of the input stage and from the time walk of the discriminator itself. The latter contribution is due to the strong dependence of the signal propagation delay, within the discriminator circuit, on the amplitude of the input differential signal. According to the specifications of the manufacturer, the output ECL signal delay increases by 50 ps when the amplitude of the input differential pulse is changed from 1 to 0.1 V. For signals lower than 0.1 V this time shift may be even larger. However, this effect should not influence the circuit performance when SPADs with uniform breakdown are operated by fast AQCs. In fact the avalanche current of a SPAD has a standard amplitude, since it always reaches a steady value given by the ratio between the excess bias above V_b and the diode series resistance. Provided that the driver of the AQC resets the detector bias voltage swiftly and smoothly, the probability for a photon to arrive when the SPAD bias is not yet settled becomes negligible. Therefore, in practice the only cause of electronic jitter of the AQC remains the noise of the input stage.

Figure 3 illustrates the link between the noise at the input of the discriminator and the resulting timing jitter. Let us consider the signal at the noninverting input of the fast discriminator. The static bias of the inverting input node is represented in Fig. 3 by the dashed line and defines the discriminator threshold level, V_{th}. In the absence of noise, the

threshold crossing time would be well defined, but if a voltage noise with a root mean square amplitude equal to σ_v is superimposed on the signal, the crossing time jitters. Straightforward geometry gives the root mean square σ_t of the resulting timing jitter as

$$\sigma_t = \frac{\sigma_v}{F}, \tag{1}$$

where F is the average slope of the voltage signal at threshold crossing. Since the discriminator is a differential amplifier with a 300 MHz bandwidth,[11] the variance σ_v^2 of the voltage noise at the discriminator inputs can be estimated by integrating the voltage noise power spectrum due to the components of the input stage of the AQC over an equivalent bandwidth of $\Delta f = 300$ MHz.

The overall effect of the various noise sources can be represented by a voltage noise source, S_v, in series to each input of the discriminator and a current noise source, S_I, in parallel to each resistance R.

The only contribution to S_v is the series equivalent noise source of the discriminator S_v^d, while S_I is the sum of three terms:

(a) the parallel equivalent noise source of the discriminator, with power spectrum S_I^d;
(b) the current noise spectrum of R, given by $4kT/R$, that is 3.2×10^{-22} A^2/Hz for $R = 51\ \Omega$;
(c) the noise due to T_1 and the other components, which can be represented with a source of current noise connected in parallel to R, with a power spectrum S_I^{net}.

Therefore the overall current noise power spectrum at the noninverting discriminator input is given by

$$S_I = S_I^d + \frac{4kT}{R} + S_I^{\text{net}}. \tag{2}$$

The same expression holds for the current noise of the branch connected to the inverting discriminator input. From straightforward noise calculations a value of 0.8×10^{-22} A^2/Hz is estimated for S_I^{net}. Regarding S_I^d, this spectral density is expected to be orders of magnitude lower, since it is mainly due to the input bias current of the discriminator, which is in the nA range. In order to directly assess the value of these noise sources and their effect on timing performance, we have carried out the measurements discussed in the next section.

IV. NOISE MEASUREMENTS

The measurement of the timing jitter introduced by the AQC may be performed by collecting a histogram of the time delay between the electrical signal of a wave form generator, which triggers the AQC, and the AQC output. In this experimental setup the start input of a TPHC is triggered by an electrical signal synchronous with the generator output. Usually this signal is shaped from an auxiliary output of the wave form generator module in order to match the NIM standard pulse required by the TPHC inputs. The AQC output is instead readily available for the stop input of the TPHC. The FWHM of the histogram collected with the MCA is given by

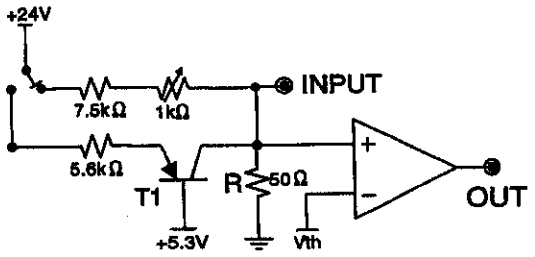

FIG. 4. Simplified circuit for noise measurements. The signal is injected directly into the noninverting input of the discriminator; measurements have been performed in both conditions of transistor T_1 biased on and biased off.

$$\text{FWHM} = \sqrt{(\text{FWHM}_{\text{AQC}})^2 + (\text{FWHM}_{\text{TPHC}})^2 + (\text{FWHM}_{\text{shaper}})^2}. \tag{3}$$

In order to evaluate the contribution due to the AQC alone, the additional jitter introduced by the TPHC and by the shaper should be either negligible or separately evaluated.

In our measurements we have instead adopted a different setup. The same output pulse from the wave form generator was split and fed to the inputs of two identical trigger circuits. The output signals of these circuits, delayed with cables of suitable lengths, trigger the start and the stop input of the TPHC, respectively. In this way the FWHM of the measured histogram is now given by

$$\text{FWHM} = \sqrt{2(\text{FWHM}_{\text{AQC}})^2 + (\text{FWHM}_{\text{TPHC}})^2}. \tag{4}$$

The relative importance of the contribution due to the TPHC is reduced and additional shaping of the triggering signal for the start of the TPHC is no longer required. The contribution of the TPHC, in our case an ORTEC model 566, was checked by applying the same standard NIM pulse to both the start and the stop input: FWHM values of 7 ± 1 ps were found for counting times up to 10 min.

Instead of employing two complete AQCs, two simpler circuits were mounted according to the scheme of Fig. 4. They are a replica of the branch of the AQC input stage that receives the current signal coming from the detector. The inverting input of the comparator is held at a constant bias voltage, thus defining the threshold.

By comparing Fig. 4 with Fig. 2 one can note that the diodes D_1 and the 12 kΩ resistance were not introduced, while there are two additional components, the 7.5 kΩ resistance and the 1 kΩ trimmer. These changes are not expected to affect the significance of the measurements, since it will be seen in the following that the noise due to these components is negligible with respect to the noise of the discriminator itself and of the common base transistor. The circuit of Fig. 4 makes possible the injection of a pulse from a wave form generator directly at the noninverting input of the discriminator. The circuit can work with the transistor T_1 either biased off or biased on in common base configuration. When T_1 is set off the trimmer is adjusted to restore the correct bias at the discriminator input.

Since R is much lower than the 60 kΩ input resistance of the discriminator, the variance of the voltage noise at the noninverting input is

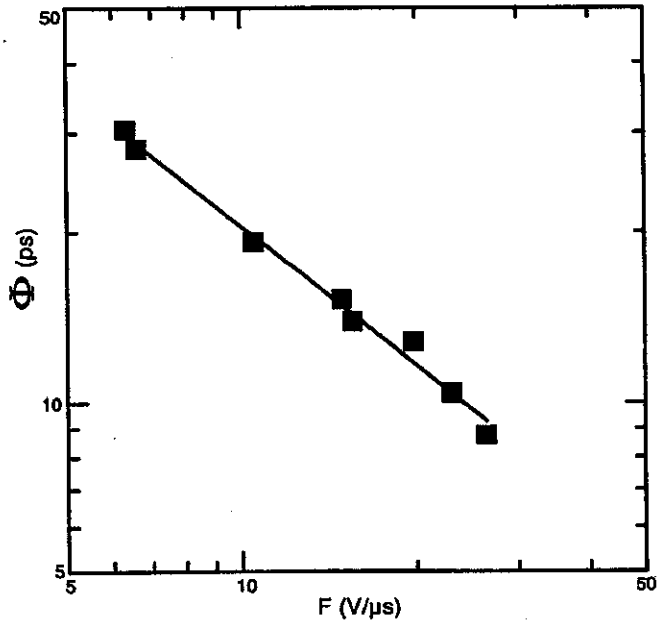

FIG. 5. Experimental results of time jitter measurements performed with the circuit of Fig. 4 working with T_1 off. On the vertical axis we have plotted the quantity Φ=FWHM/$\sqrt{2}$ in order to account for the jitter of only one circuit.

$$e_n^2=\left[2S_v^d+\left(S_I^d+\frac{4kT}{R}+S_I^{\text{net}}\right)R^2\right]\Delta f, \tag{5}$$

where Δf=300 MHz is the noise bandwidth and R=51 Ω. When T_1 is off, $S_I^{\text{net}}=0$. The factor 2 before S_v^d corresponds to the presence of two voltage noise generators, one at each input of the discriminator, both contributing to the noise on the differential signal. According to Eqs. (1) and (4) the FWHM of the measured time jitter is

$$\text{FWHM}=2.35\sqrt{\sigma_t^2}=2.35\sqrt{2\frac{e_n^2}{F^2}+\sigma_{\text{TPHC}}^2}, \tag{6}$$

where F is the average slope at threshold crossing of the voltage signal on the 51 Ω load. In Eq. (6) we have assumed a 2.35 ratio between the FWHM and the root mean square, as it is in the case of Gaussian distributions. Figure 5 shows the experimental results obtained working with T_1 off, compared with a curve fitted according to Eq. (6). More precisely, on the vertical axis we have plotted the quantity Φ=FWHM/$\sqrt{2}$ in order to account for the jitter of only one channel. On the horizontal axis is the signal slope, F. Both the scales are logarithmic. The fitted curve is a straight line with a −45° slope, which confirms that the contribution σ_{TPHC}^2 is practically negligible [see Eq. (6)].

When the transistor T_1 is turned on, the time jitter increases only very slightly. Since the only difference with respect to the previous set is the presence of S_I^{net}, we conclude that the contribution of this term to the noise, and hence to the FWHM, is almost negligible. Consequently, the contribution of S_I^d, which is much smaller than S_I^{net}, is completely negligible. In other terms, the experimental data point out that the dominant noise source is the series noise of the discriminator, S_v^d. By taking $\sigma_{\text{TPHC}}^2=(2.9\text{ ps})^2$, $S_I^{\text{net}}=0.8\times10^{-22}$ A²/Hz and $4kT/R=3.2\times10^{-22}$ A²/Hz for R=51 Ω, the experimental data are well fitted by Eq. (6) assuming $S_v^d=20\times10^{-18}$ V²/Hz.

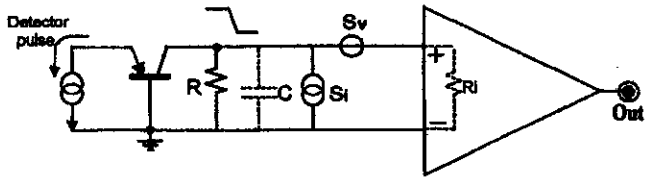

FIG. 6. Small signal circuit of the AQC input branch with the equivalent noise sources.

This quantitative result suggests that the simplest way to reduce the time jitter is to increase the R value. In fact by increasing R the signal slope is increased while the total noise is only slightly affected. However, as outlined in Fig. 6, the increase of the signal slope is limited at high R values by the capacitance C between the noninverting input and ground. Therefore the presence of an optimum R value is expected.

In Fig. 6, R_i=60 kΩ is the input resistance of the fast discriminator, while the input common-base transistor is characterized by a 450 ps transit time. The shape of the voltage signal at the discriminator input and the threshold crossing slope can be accurately computed by detailed circuit analysis of the network in Fig. 6 starting from the amplitude and the slope of the avalanche current pulse. The optimum R value can thus be identified. We found, however, that the same results can be obtained by a simplified analysis, which is here reported. Working with ultrafast SPADs biased at optimum timing performance, the avalanche current has an amplitude from 1 to 2 mA and a leading edge slope from 0.2 to 0.4 mA/ns. Therefore the avalanche current pulse can be simply modeled by a quasistep signal with a leading edge rising with a constant slope A over a duration T_0. It is assumed that this current wave form is not modified by the common-base transistor and is injected on the R-C integrator cell, characterized by time constant $\tau=RC$. Therefore, the shape of the voltage signal at the discriminator input is

$$\begin{aligned}&\frac{A}{C}\left[\tau(t-\tau)+\tau^2\exp\left(-\frac{t}{\tau}\right)\right]\quad\text{for } 0<t<T_0,\\&\frac{A}{C}\left[\tau T_0+\tau^2\exp\left(-\frac{t}{\tau}\right)\left(1-\exp\left(\frac{T_0}{\tau}\right)\right)\right]\quad\text{for } t>T_0,\end{aligned} \tag{7}$$

which is approximately a linear ramp signal delayed by τ. The time derivative of this signal is

$$\begin{aligned}&\frac{A}{C}\tau\left[1-\exp\left(-\frac{t}{\tau}\right)\right]\quad\text{for } 0<t<T_0,\\&-\frac{A}{C}\tau\left[1-\exp\left(\frac{T_0}{\tau}\right)\right]\exp\left(-\frac{t}{\tau}\right)\quad\text{for } t>T_0.\end{aligned} \tag{8}$$

The maximum derivative $F_{\max}$ occurs at $t=T_0$:

$$F_{\max}=\frac{A}{C}\tau\left[1-\exp\left(-\frac{T_0}{\tau}\right)\right], \tag{9}$$

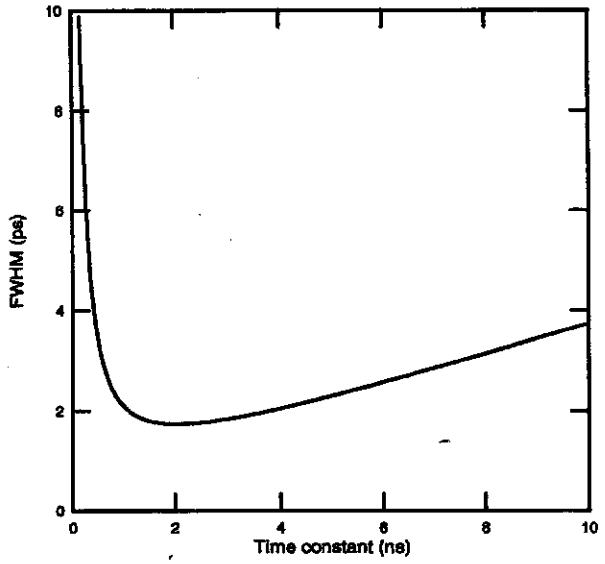

FIG. 7. Time jitter of the AQC as a function of the discriminator input time constant.

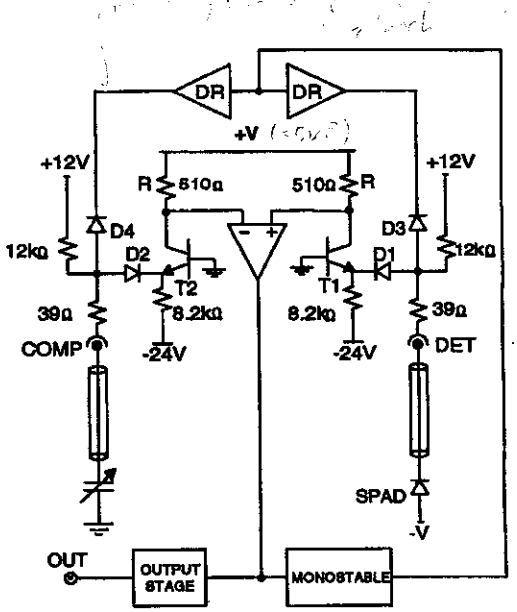

FIG. 8. Modified AQC with new input stage. The driver (DR) is a discrete push–pull stage. The previous discriminator SP9685 has been replaced by the AD96685.

which is the maximum slope of the voltage signal at the noninverting input of the discriminator. The minimum time jitter is obtained by setting the discriminator threshold so that crossing occurs at this maximum slope, that is at $t=T_0$.

Regarding the noise, as long as R is very small with respect to $R_i=60$ kΩ, the variance of the voltage noise follows the dependence of Eq. (5), therefore, the corresponding time jitter is given by

$$(\mathrm{FWHM})_{\mathrm{AQC}}=2.35\,\frac{\sigma_v}{F_{\max}}=2.35\,\frac{\sqrt{\left[2S_v^d+\frac{2S_I}{C^2}\,\tau^2\right]\Delta f}}{\frac{A}{C}\,\tau\left[1-\exp\left(-\frac{T_0}{\tau}\right)\right]} \tag{10}$$

with $S_I=4kT/R+S_I^{\mathrm{net}}=4kTC/\tau+S_I^{\mathrm{net}}$. Figure 7 shows the curve given by Eq. (10) with $A=0.4$ mA/ns and $C=4$ pF. Since, the bandwidth of the common-base transistor is large enough with respect to the rise time of the detector signal, the curve given by Eq. (10) is the same as the result of the detailed analysis. The minimum of Eq. (10) occurs near $\tau=2$ ns, which corresponds to $R=510$ Ω. An optimum threshold of 158 mV is computed from Eq. (9).

The shape of the curve can be easily interpreted. By increasing the R value, the slope of the voltage signal at the noninverting discriminator input increases and the time jitter correspondingly decreases. However the dominant current noise S_I^{net} contributes to the noise with a voltage power spectrum given by $S_I^{\mathrm{net}}R^2$. When this contribution becomes comparable to S_v^d the time jitter reaches its minimum value. A further increase of R causes a greater increase of the voltage noise than that of the signal slope, thus worsening the time jitter. Regarding the C value, it is quite clear that the minimum jitter is obtained by keeping the capacitance to the minimum value set by the parasitics. In fact the increase of C decreases the slope of the voltage signal at the discriminator input without significantly affecting the noise power.

V. IMPROVED CIRCUIT AND RESULTS

The results of the noise analysis led us to modify the input stage of the AQC according to the scheme of Fig. 8.

The value of R has been increased from the previous 51 to 510 Ω, which gives the optimum time constant of about 2 ns on the input stray capacitance of 4 pF. We have also used two n-p-n transistors (T_1, T_2) for the common-base stage, with a transition frequency of 2 GHz. In this way the circuit inputs (DET and COMP) have quiescent bias of 0 V, and the reverse voltage across the detector is given only by the value of the voltage source connected to the anode of the SPAD. Instead, in the circuit of Fig. 2 the detector reverse bias was given by the sum of the external bias source and the quiescent bias of about 6.7 V of the circuit inputs DET and COMP. This circuit modification implies a common mode voltage of 4 V at the discriminator inputs. According to the manufacturer's specifications, the performance of the discriminator is not adversely affected by this common mode voltage and this was verified in our tests. The last difference with respect to the circuit of Fig. 2 is that the bias current through the diodes D_1 and D_2 has been decreased from 3 to 1 mA. At the operating bias, the SPAD current exceeds 1 mA and the diode D_1 is turned off, thus limiting the amplitude of the voltage signal at the noninverting input to a standard 500 mV level. This is a further care in order to avoid any contribution of the discriminator time walk to the circuit jitter, since the amplitude of the detector pulses at the discriminator inputs is always the same, even if the detector is triggered when its bias has not been perfectly restored.

The improved performance of the new circuit has been verified by carrying out measurements identical to those described in Sec. IV. The only difference was that two complete AQCs were used instead of the simplified circuits of Fig. 5. Figure 9 shows the dependence of the circuit jitter as a function of the leading edge slope of the detector pulse for

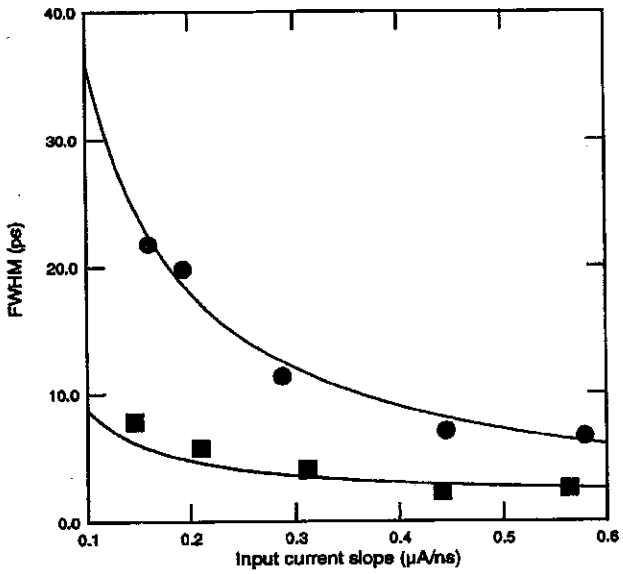

FIG. 9. AQC time jitter as a function of the leading edge slope of the input current signal. The lines are obtained from Eq. (10), the upper one for $R=51$ Ω, the lower for $R=510$ Ω. Experimental results are represented with dots for the old circuit, with squares for the new one.

both the former and the improved AQCs. The solid lines are the theoretical values obtained on the basis of Eq. (10), while dots and squares are the experimental results. In Fig. 9 we report the contribution to the FWHM jitter only due to one AQC, obtained from Eq. (4) by quadratically subtracting the contribution of the TPHC. Note that the new circuit has a jitter always lower than 10 ps FWHM when triggered by signals from fast SPADs. Recently the fast discriminator SP9685 has been replaced on the shelves by the component AD96685.[13] This component features lower power consumption, higher input resistance ($R_i=200$ kΩ), and a slightly lower input capacitance ($C=3$ pF) but at the expense of a longer propagation delay (2.5 ns). We have verified that with the new discriminator the circuit performance remains practically the same.

In conclusion the picosecond timing performance of the fastest SPADs can be fully exploited only with an accurate design of all the detector electronics. The quenching circuit, which directly drives the photodiodes and collects its current signal, is one of the most critical parts of the TCPC setup. In this paper we have discussed the input stage of AQCs capable of driving the detector in a remote position, connected to the electronics by a coaxial cable. An experimental analysis of the circuit noise has led to a new improved AQC which features a time jitter better than 10 ps, well below the intrinsic time jitter of the fastest SPADs nowadays available.

ACKNOWLEDGMENTS

The work has been supported by MURST (The Italian Ministry of University) and by CNR (Italian National Research Council). We wish to thank S. Vanoli and S. Masci for their technical support in measurements and circuit testing.

[1] M. Ghioni and G. Ripamonti, Rev. Sci. Instrum. **62**, 163 (1991).
[2] L. Li and L. M. Davis, Rev. Sci. Instrum. **64**, 1524 (1993).
[3] S. Cova, A. Longoni, and A. Andreoni, Rev. Sci. Instrum. **52**, 408 (1981).
[4] S. Cova, M. Ghioni, F. Zappa, and A. Lacaita, Rev. Sci. Instrum. **64**, 118 (1993)
[5] S. Cova, A. Lacaita, M. Ghioni, G. Ripamonti, and T. Louis, Rev. Sci. Instrum. **60**, 1104 (1989).
[6] Hamamatsu Photonics K.K., Hamamatsu City, Japan, and Hamamatsu Corp., Bridgewater, N.J. MCP PMTs data sheets and Technical Information No. ET-03/Oct. 1987.
[7] M. Ghioni, S. Cova, and C. Samori, Rev. Sci. Instrum. (submitted).
[8] S. Cova, A. Longoni, and G. Ripamonti, IEEE Trans. Nucl. Sci. **NS-29**, 599 (1982).
[9] P. Antognetti, S. Cova, and A. Longoni, Proceedings of the Ispra Nuclear Electronics Symposium, 1975, Euratom Publication EUR 537e (unpublished), p. 453.
[10] S. Cova, US. Patent No 4,963,727, Italian Patent No 22367A/88. Industrial licence to SILENA S.p.A. Milano, Italy.
[11] Ultrafast Comparators SP9685, High Speed Data Processing, Integrated Circuit Handbook, Plessey Semiconductors Ltd., Cheney Manor, Swindon, Wiltshire, UK, Publication No. P.S. 1989, December 1983.
[12] A. Lacaita, P. A. Francese, F. Zappa, and S. Cova, Appl. Opt. **33**, 6902 (1994).
[13] Ultrafast Comparators AD96685, Analog Device Inc. P. O. Box 9106, Norwood, MA, U.S.A. Linear Product Databook, p. 3–17, April 1988.